Int J Fract
https://doi.org/10.1007/s10704-022-00640-4

ORIGINAL PAPER

Effects of diffusion and primary creep on intergranular cavitation at high temperatures

John W. Sanders · Niloofar Jamshidi · Negar Jamshidi · Mohsen Dadfarnia · Sankara Subramanian · Huseyin Sehitoglu · James Stubbins · Petros Sofronis

Received: 16 August 2021 / Accepted: 27 April 2022

Abstract Next-generation reactors are expected to play a crucial role in power production in the foreseeable future. Due to the extreme anticipated operating temperatures of next-generation plants, a major concern for candidate materials is failure by creep cavitation. Indeed, many commonly used component lifetime estimates are based on how quickly intergranular voids grow. Void growth is known to be caused by three processes: diffusion along the void surface, diffusion along the grain boundary, and creep of the surrounding grains. However, until now, previous creep cavitation models have neglected to account explicitly for both the surface diffusion process and primary creep effects. More precisely, previous models assume that surface diffusion occurs rapidly enough to sustain quasi-equilibrium void growth, and that the creep response of the grains is accurately modeled by power-law secondary creep. To illustrate the potential ramifications of these assumptions, we present here novel finite element simulations of intergranular void growth under the combined effects of surface diffusion, grain boundary diffusion, and bulk primary/secondary creep. Our results indicate that crack-like void growth may be more prevalent at high temperatures than previously assumed, and that void growth of any kind is substantially accelerated during the primary creep regime. This could have serious implications for previous creep rupture models, which may underestimate the rate of void growth by almost two orders of magnitude or more. Based on our results, we establish quantitative criteria for quasi-equilibrium and crack-like void growth, and we suggest quantitative improvements to the existing models.

Keywords Cavitation · Creep · Diffusion · Fracture · Grain boundaries

J. W. Sanders (✉) · N. Jamshidi · N. Jamshidi
Department of Mechanical Engineering, California State University, Fullerton, 800 North State College Boulevard, Fullerton, CA 92831, USA
e-mail: jwsanders@fullerton.edu

M. Dadfarnia
Department of Mechanical Engineering, Seattle University, 901 12th Street, Seattle, WA 98122, USA

S. Subramanian
PhotoGAUGE, 13A/209, Velachery Main Road, Chennai 600042, India

H. Sehitoglu · P. Sofronis
Department of Mechanical Science and Engineering, University of Illinois at Urbana-Champaign, 1206 West Green Street, Urbana, IL 61801, USA

P. Sofronis
e-mail: sofronis@illinois.edu

J. Stubbins
Department of Nuclear, Plasma, and Radiological Engineering, University of Illinois at Urbana-Champaign, 216 Talbot Laboratory, 104 South Wright Street, Urbana, IL 61801, USA

1 Introduction and literature review

At present, nuclear power remains one of the most viable carbon-neutral energy sources, and Generation-

Published online: 19 May 2022

IV nuclear reactors will play a major role in power production in the foreseeable future (GEN IV International Forum 2020; World Nuclear Association 2020). Several Generation-IV reactor designs have been proposed, all of which will operate at higher temperatures than today's reactors, including: Gas cooled fast reactors (850 °C), Lead cooled fast reactors (480–570 °C), Molten salt reactors (700–800 °C), Supercritical water cooled reactors (510–625 °C), Sodium cooled fast reactors (500–550 °C), and Very high temperature gas reactors (750–1000 °C) (Chersola et al. 2015; GEN IV International Forum 2020; World Nuclear Association 2020). Such high temperatures promise increased thermal efficiency compared to current energy conversion systems and have the potential to facilitate the production of hydrogen gas for a hydrogen economy. However, these conditions will also place a severe burden on plant components—particularly the Intermediate Heat Exchanger. Indeed, the GEN-IV International Forum 2020 Annual Report states that one of the primary challenges for Generation-IV structural materials is "time-dependent failure and microstructural instability in operating environments" (i.e., creep rupture), and that "multi-scale modelling is needed to support improved design methods" (GEN IV International Forum 2020). The present work aims to contribute to this much-needed multi-scale modeling.

High-temperature creep rupture is known to be controlled by intergranular cavitation: the nucleation, growth, and coalescence of voids along grain boundaries (Argon 1982). This fact has been established based on decades of experiments on a myriad of structural metals (Argon 1982; Pataky et al. 2013; Tung et al. 2014). Accordingly, in an effort to anticipate and predict rupture, mathematical void growth models have been developed based on the underlying physics of the cavitation process.

The seminal work of Hull and Rimmer (1959) was one of the first to suggest that the diffusion of matter plays a significant role in bringing about void growth, with atoms migrating along the void surface (a process henceforth referred to as "surface diffusion") and along the grain boundary (henceforth "grain boundary diffusion"). It is now well known that the relative magnitudes of surface and grain boundary diffusion determine the shape assumed by a growing void. When surface diffusion occurs much more rapidly than grain boundary diffusion, a void maintains its original shape as it grows, and this is referred to as "quasi-equilibrium

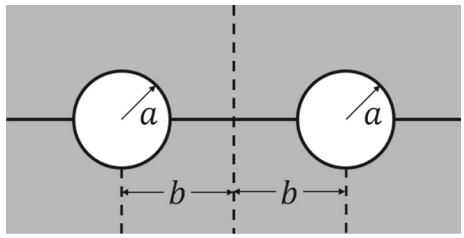

Fig. 1 Two adjacent intergranular voids. The mean void radius is a, and the center-to-center void spacing is $2b$

void growth." Conversely, when grain boundary diffusion occurs much more rapidly than surface diffusion, the void elongates along the direction of the grain boundary, a process referred to as "crack-like void growth" (Chuang et al. 1979; Chuang and Rice 1973; Kagawa 1976). Hull and Rimmer (1959) were also among the first to estimate the rupture time of a specimen or component based on the rate at which voids grow. One expects voids to grow until the grain boundary ligament between two adjacent voids can no longer support the local stresses, at which point the ligament fails and a microcrack is born. As illustrated in Fig. 1, denote by a the mean void radius and by $2b$ the center-to-center void spacing, and suppose that the ligament will fail when $a = \lambda b$, where $\lambda \in (0, 1]$. Then, according to Hull and Rimmer (1959), we may estimate the rupture time as

$$t_r = \int_{a_0}^{\lambda b} \frac{da}{\dot{a}}, \tag{1}$$

where a_0 is the initial void radius, a superscribed dot denotes differentiation with respect to time, and it is understood that $\dot{a}$ is a function of the system parameters (including the current void radius a). Naturally, the rupture time scales with the reciprocal of the void growth rate $\dot{a}$, since faster void growth leads to shorter rupture times, and vice versa. The functional form of $\dot{a}$ can be deduced from the results of void growth simulations, and over the last several decades a great deal of effort has been devoted to accurate, physics-based models of void growth.

Kagawa (1976) and Chuang et al. (1979) were the first to investigate void growth analytically in the presence of both surface diffusion and grain boundary diffusion, allowing the shape of the void to be determined by the analysis. These authors considered both axisymmetric and cylindrical voids under remotely applied

uniaxial tension, and they treated the grains as rigid, neglecting creep deformation in the surrounding material. By linearizing the surface diffusion equation, they derived three solutions for the void profile: one for quasi-equilibrium void growth, another for crack-like void growth, and a third solution—the so-called "self-similar" solution—whose predictions agree with those of the quasi-equilibrium solution or the crack-like solution, depending on the value of a dimensionless parameter $\chi = a^3\dot{a}/\mathcal{D}_s\gamma_s$, where γ_s is the surface free energy, and $\mathcal{D}_s = D_s\delta_s\Omega/kT$ is the surface diffusivity, where $D_s\delta_s$ is the void surface diffusion coefficient, Ω is the atomic volume of the diffusion species, $k = 1.38 \times 10^{-23}$ J/K is Boltzmann's constant, and T is the absolute temperature. For small values of χ, the self-similar solution was found to agree with the quasi-equilibrium solution, and for large values of χ, it was found to agree with the crack-like solution. On the basis of their results, Chuang et al. (1979) established quantitative criteria for quasi-equilibrium void growth versus crack-like void growth of an axisymmetric void. From Kagawa's (1976) results, one can derive analogous criteria for the case of a cylindrical void. According to Kagawa's (1976) original work, quasi-equilibrium void growth should occur under remote stresses S satisfying

$$\frac{Sa}{\gamma_s} < \psi\left(1-\frac{a}{b}\right)\left[1+\frac{4}{9}\left(\frac{b}{a}-1\right)\chi_0\Delta\right], \tag{2}$$

where ψ is the angle, in radians, the void tip makes with the grain boundary ($\psi = \pi/2$ for a circular void), and $\Delta = D_s\delta_s/D_b\delta_b$ is the ratio between the surface and grain boundary diffusion coefficients. Similarly, Kagawa (1976) predicts that crack-like void growth should occur under remotely applied stresses S satisfying

$$\frac{Sa}{\gamma_s} > \psi\left(1-\frac{a}{b}\right)\left[\chi_0^{1/3}+\frac{2}{3}\left(\frac{b}{a}-1\right)\chi_0^{2/3}\Delta\right]. \tag{3}$$

The parameter χ_0 that appears in both (2) and (3) is an appropriate value for χ that describes the "cutoff" between quasi-equilibrium and crack-like void growth. On the basis of his results, Kagawa (1976) recommended taking $\chi_0 = 5$. It is worth noting that these criteria overlap, that is, there exist conditions under which (2) and (3) are satisfied simultaneously. We interpret this overlap as corresponding to void growth which is both quasi-equilibrium and crack-like (that is, something in between the two), which we will refer to as "dynamic" void growth, for reasons that will become clear in Sect. 3. It should be noted that these criteria were derived assuming rigid grains, neglecting creep of the surrounding material, and are therefore applicable only at low temperatures–not the high temperatures anticipated for Generation-IV plants. In the present work, we will establish analogous criteria for high temperatures.

Needleman and Rice (1980) were the first to study how creep deformation of the grains interacts with grain boundary diffusion to bring about void growth at high temperatures. They performed finite element simulations of axisymmetric voids in uniaxial tension under the influence of both grain boundary diffusion and bulk creep, and tabulated numerical values for the void growth rate. Needleman and Rice (1980) did not account for surface diffusion explicitly; rather, they assumed ab initio that surface diffusion occurred rapidly enough to maintain quasi-equilibrium void growth. The seminal contribution of Needleman and Rice (1980) was the introduction of a grain boundary *diffusion length*

$$L_b = \left(\frac{\mathcal{D}_b S}{\dot{\varepsilon}_\infty}\right)^{1/3}, \tag{4}$$

where $\mathcal{D}_b = D_b\delta_b\Omega/kT$ is the grain boundary diffusivity and $\dot{\varepsilon}_\infty$ is the remote creep strain rate. For remote power-law creep, $\dot{\varepsilon}_\infty = \dot{\varepsilon}_0(S/\sigma_0)^n$, where $\dot{\varepsilon}_0 = 10^{-6}$ s^{-1} is the conventional reference strain rate, σ_0 is the reference stress, and n is the creep exponent. Informally, L_b can be interpreted as the length over which grain boundary diffusion is significant. However, the true usefulness of L_b lies in the dimensionless ratio L_b/a, which gives a measure of the relative importance of grain boundary diffusion vis-à-vis bulk creep. When this ratio is large (typically 20 or greater), grain boundary diffusion is more significant than bulk creep in bringing about void growth, and when this ratio is small (typically 4 or less), bulk creep is more significant than grain boundary diffusion. For intermediate values, the effects of grain boundary diffusion and bulk creep are comparable. The interplay between the creep and diffusion processes can have a significant effect on rupture time (Sanders et al. 2017).

Virtually all subsequent void growth modeling has been based on the extension of the Needleman and Rice (1980) model to multiaxial stress states (Sham and Needleman 1983; Van der Giessen and Tvergaard 1996; Van der Giessen et al. 1995) and internal void pressures (Van der Burg and Van der Giessen 1996a, b, 1997; Van der Burg et al. 1996). Budiansky et al. (1982) devel-

oped analytical expressions for the void growth rate under the influence of bulk creep by itself. Sham and Needleman (1983) then extended the work of Needleman and Rice (1980) to multiaxial stress states, proposing a closed-form expression for the void growth rate that approximated their numerical results by stitching together the analytical expressions of Chuang et al. (1979) [modified according to an observation by Chen and Argon (1981)] and Budiansky et al. (1982). Sham and Needleman's (1983) expression was developed for low porosities (a/b) and high stress triaxialities. Van der Giessen and Tvergaard (1996) and Van der Giessen et al. (1995) then extended the results of Sham and Needleman (1983) to lower triaxialities by stitching on additional expressions due to Tvergaard (1984a, b, 1986), and to higher porosities by incorporating additional expressions of their own.

Once the void growth rate $\dot{a}$ has been established, one may estimate the time to initial rupture using (1). Equivalently, one may consider that rupture initiates when the porosity a/b at any given point reaches a critical value $\lambda \in (0, 1]$ (Huang et al. 2021). This scheme has provided the basis for many commonly used creep rupture models and lifetime estimates up to the present day. For example, Wen et al.'s (2017, 2018) employ the Van der Giessen and Tvergaard (1996) and Van der Giessen et al. (1995) void growth model as part of the constitutive behavior for their finite element simulations of creep crack propagation under both monotonic and cyclic loading. In Wen et al.'s (2017, 2018) simulations, a uniform mesh of square quadrilateral elements is placed ahead of the initial crack tip, with each quadrilateral element further subdivided into four constant-strain triangular sub-elements. The stiffness of a quadrilateral element is made to vanish when the porosity a/b [or, using Wen et al.'s (2017, 2018) notation, r/b] reaches a critical value of 0.95 in at least two of the four triangular sub-elements, thus simulating local material failure and crack growth. Even more recently, Rovinelli et al. (2021) and Bieberdorf et al. (2021) have employed the Van der Giessen and Tvergaard (1996) and Van der Giessen et al. (1995) void growth model to simulate damage in the context of their own finite element simulations.

The aforementioned void growth models are also used to simulate failure by creep rupture in the presence of high temperature hydrogen attack (HTHA). Notably, Van der Burg and Van der Giessen (1996a, b, 1997) and Van der Burg et al. (1996) further extended the Van der Giessen and Tvergaard (1996) and Van der Giessen et al. (1995) void growth model to account for an internal pressure distribution (e.g., due to methane gas) on the void surface. See recent work by Dadfarnia et al. (2019) simulating hydrogen attack in carbon steels under constrained void growth.

Crucially, we observe that every one of the works cited above only accounts for at most two of the three fundamental void growth mechanisms at a time—those being surface diffusion, grain boundary diffusion, and bulk creep. Most notably, Needleman and Rice (1980) did not model the surface diffusion process explicitly, instead assuming that surface diffusion occurred rapidly enough to maintain quasi-equilibrium void growth. Furthermore, although Needleman and Rice (1980) considered creep of the grains, they modeled the constitutive behavior of the bulk using the classical power-law creep model, which only applies in the secondary creep phase. As a result, all existing creep cavitation models that are based on the extension of Needleman and Rice (1980) to higher triaxialities (Bieberdorf et al. 2021; Rovinelli et al. 2021; Sham and Needleman 1983; Van der Giessen and Tvergaard 1996; Van der Giessen et al. 1995; Wen et al.'s 2018, 2017) and internal void pressures (Dadfarnia et al. 2019; Van der Burg and Van der Giessen 1996a, b, 1997; Van der Burg et al. 1996) suffer from two inherent limitations: (1) they can neither anticipate nor simulate crack-like void growth, and (2) they cannot capture the effects of primary creep when it is present (for the importance of modeling primary creep as it pertains to nuclear power plant components, see for example Robinson et al. (1976)). For the sake of brevity, such models will henceforth be referred to as the "previous models." [For a discussion of void growth models that are *not* based on Needleman and Rice (1980)—which are not directly relevant to the present work but may nevertheless be of interest to some readers—the reader is referred to a recent survey of cavitation models by Sui et al. (2022)].

To investigate the potential ramifications of the aforementioned limitations, the present authors have developed a finite element code capable of simulating the growth of a single intergranular void under the combined effects of surface diffusion, grain boundary diffusion, and bulk primary/secondary creep (with a smooth transition between primary and secondary creep). The first simulation results obtained using this code were reported in Sanders et al. (2021) for material parameters representative of 2 1/4 Cr-1 Mo Steel

(a high-temperature alloy used in liquid metal cooled fast breeder reactor components) at 566 °C. However, there were not yet enough results to make general conclusions at that time. In the present work, we extend our previous results (Sanders et al. 2021) in order to establish approximate, closed-form criteria for quasi-equilibrium and crack-like void growth—analogous to Kagawa's expressions given by (2) and (3)—for a wide range of realistic model parameters. We will also present the very first simulation results for the mass flux along the void surface and the grain boundary. So that our results may generalize to other materials and temperatures, we will express all results in terms of suitable dimensionless groups. As noted in Sanders et al. (2021), when surface diffusion is present, we may define a surface diffusion length $L_s = (\mathcal{D}_s S/\dot{\varepsilon}_\infty)^{1/3}$, analogous to the grain boundary diffusion length of Needleman and Rice (1980). In that case, straightforward dimensional analysis on the system parameters $a_0, b, \mathcal{D}_s, \mathcal{D}_b, \dot{\varepsilon}_\infty, \gamma_s, S$, and ψ yields five independent dimensionless groups:

$$\frac{1}{a_0}\left(\frac{\mathcal{D}_b S}{\dot{\varepsilon}_\infty}\right)^{1/3}, \quad \frac{1}{a_0}\left(\frac{\mathcal{D}_s S}{\dot{\varepsilon}_\infty}\right)^{1/3}, \quad \frac{S a_0}{\gamma_s}, \quad \frac{a_0}{b}, \quad \text{and} \quad \psi. \tag{5}$$

The first two groups are the normalized grain boundary and surface diffusion lengths L_b/a_0 and L_s/a_0, respectively. The remaining groups appeared in Kagawa's (1976) criteria for quasi-equilibrium and crack-like void growth, as given by (2) and (3). The diffusion lengths also appeared in Kagawa's criteria, but only through their ratio, since $\Delta = (L_s/L_b)^3$. In fact, we will show that, for a wide range of realistic parameters, the void shape still depends on L_s and L_b only in their ratio, even when creep is accounted for.

The remainder of this paper is organized as follows. We begin Sect. 2 by formulating the initial-boundary-value problem of a cylindrical void in a creeping material, accounting explicitly for both surface diffusion and grain boundary diffusion. In Sect. 3, we present the results of an extensive parameter study on the dimensionless quantities L_b/a_0, L_s/a_0, and Sa_0/γ_s. To see the effects of primary creep, we employ a unified creep-plasticity model due to Robinson et al. (1976), which captures both primary creep and secondary creep, with a smooth transition in between. Based on our results, we develop quantitative criteria for quasi-equilibrium and crack-like void growth, and compare our criteria to those of Kagawa (1976) given in (2) and (3). In Sect. 4, we conclude the paper by discussing potential ramifications for previous creep cavitation models, and we make some suggestions for how to improve those models when possible.

2 Problem formulation

As in Sanders et al. (2021), we consider an array of intergranular voids, each initially circular in profile ($\psi = \pi/2$) and of radius a_0, with an initial center-to-center spacing of $2b$. Following Kagawa (1976) and Chuang et al. (1979), we consider cylindrical voids which are very long in the out-of-plane direction, and we restrict attention to a square unit cell, of initial width and height each equal to $2b$, centered on a single void. This unit cell is subjected to a remotely applied uniaxial stress S perpendicular to the grain boundary. Due to the symmetry of the geometry and the applied loads, it suffices to consider only one quarter of the unit cell, as shown in Fig. 2a, in which the grain boundary is aligned along the x-axis.

The bulk material, denoted here by A, is modeled as an incompressible solid subjected to the following boundary conditions. By symmetry, the material along the y-axis in Fig. 2a is constrained against movement in the x -direction. Along the top edge of the unit cell (denoted here by S_T), the material is subjected to a uniform and constant tensile stress S corresponding to the remotely applied load. Furthermore, S_T is constrained to remain horizontal at all times. The right edge of the unit cell is taken to be traction-free, and is constrained to remain vertical at all times.

Denote by S_s the surface of the void, which extends from point B to point C in Fig. 2a. This surface is subjected to an outward normal stress $\gamma_s\kappa$ due to surface tension, where γ_s is the surface free energy and κ is the curvature of the void surface (Chuang et al. 1979). Due to chemical potential gradients, matter diffuses along the void surface and is deposited along S_s. Let j_s denote the volumetric flux (i.e., the volume of matter diffused per unit out-of-plane length per unit time) along the void surface, and let α be the thickness of matter deposited *onto* the void surface by this process (note that, when $\alpha < 0$, matter is depleted from the

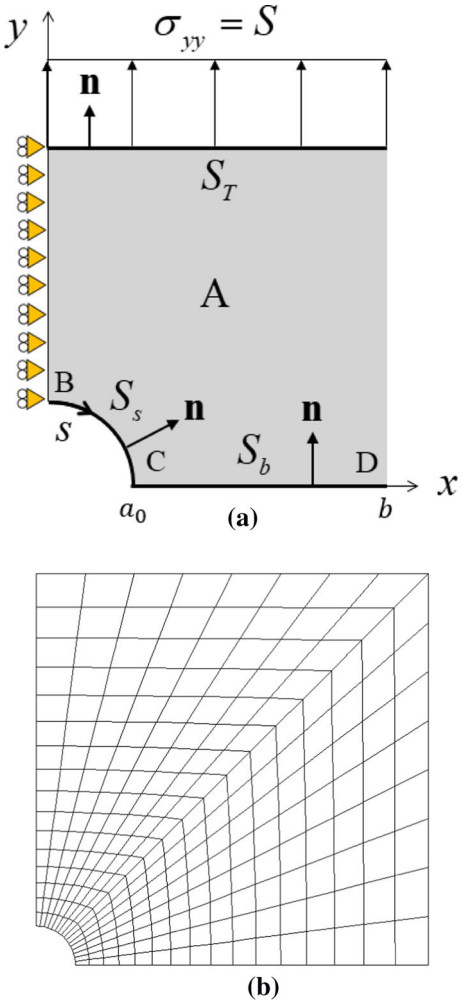

Fig. 2 **a** Quarter unit cell model of an intergranular void. **b** Finite element mesh used in the present work

void surface). The conservation of mass dictates that

$$\frac{d j_s}{ds} + \dot{\alpha} = 0 \quad \text{along } S_s, \tag{6}$$

where s is the arc length along S_s, starting from zero at point B, and j_s is taken to be positive in the direction of increasing s. Along S_s, the chemical potential is given by $\mu(s) = \mu_0 - \Omega\gamma_s\kappa(s)$, where $\gamma_s\kappa(s)$ is the work required to deposit matter against the normal stress, Ω is the atomic volume, and μ_0 is the reference chemical potential in the bulk. According to Fick's law,

$$j_s = -\frac{D_s\delta_s}{kT}\frac{d\mu}{ds} = \mathcal{D}_s\gamma_s\frac{d\kappa}{ds} \quad \text{along } S_s, \tag{7}$$

where $\mathcal{D}_s$ is the surface diffusivity (defined previously in Sect. 1), and it is assumed that γ_s is uniform. By symmetry, the flux should vanish at the top B of the void: $j_s(0) = 0$.

Similarly, denote by S_b the grain boundary, which extends from point C to point D in Fig. 2a. Matter arriving by surface diffusion is deposited on, and continues to diffuse along, the grain boundary. Let j_b denote the volumetric flux along the grain boundary (taken positive in the direction of increasing s, where s continues where it left off at point C). Following Needleman and Rice (1980), we assume that there is no grain boundary sliding or cracking, so that the rate at which matter is deposited onto the grain boundary coincides with the normal velocity v_n of the grain boundary surface. In this way, the conservation of mass requires that

$$\frac{d j_b}{ds} + v_n = 0 \quad \text{along } S_b, \tag{8}$$

where we are employing the convention that the normal directions to the void surface and grain boundary point *into* the surrounding material, in order to maintain consistency with Needleman and Rice (1980) (see Fig. 2a). Along S_b, the chemical potential is given by $\mu(s) = \mu_0 - \Omega\sigma_n(s)$, where σ_n is the tensile stress normal to the grain boundary, and the second term represents the work required to deposit matter against σ_n. Fick's law states that

$$j_b = -\frac{D_b\delta_b}{kT}\frac{d\mu}{ds} = \mathcal{D}_b\frac{d\sigma_n}{ds} \quad \text{along } S_b, \tag{9}$$

where $\mathcal{D}_b$ is the grain boundary diffusivity (defined previously in Sect. 1). By symmetry, the flux should vanish at the edge D of the unit cell: $j_b(s_D) = 0$. At point C, where the void surface meets the grain boundary, the flux and the chemical potential must be continuous. That is, $j_s(s_C) = j_b(s_C)$ and $\sigma_C = \gamma_s\kappa_C$, where σ_C is the stress normal to the grain boundary at C, and κ_C is the curvature of the void surface at C.

As noted above, the displacement by which the grains separate along S_b is related to the amount of matter deposited along the grain boundary in a relatively straightforward manner. Specifically, at any point along the grain boundary, the normal velocity v_n happens to be identical to the rate at which matter is deposited there, and that allows us to write (8) in terms of v_n. This constraint arises from the assumption that there is no grain boundary sliding or cracking. However, the void surface is not similarly constrained. Indeed, the void surface is free to deform due to the applied tractions in addition to matter deposition. As a result, (6) must be written not in terms of the normal velocity of

the void surface, but rather in terms of the rate $\dot{\alpha}$ at which matter is deposited along the void surface, and the amount of matter α that has been deposited on the surface must be treated as a kind of state variable.

To handle the added complication of surface diffusion, we employ a similar numerical approach to Subramanian and Sofronis (2002) [see also Pan and Cocks (1995)], such that at each time step matter deposition along the void surface is treated separately from the other deformation. In particular, we decompose the displacement of the void surface as $u_i^s = u_i^0 - \alpha n_i$, where u_i^0 is the "baseline" displacement of the void surface arising from processes other than surface diffusion, α is the thickness of matter that has accumulated on the void surface, and n_i is the inward unit normal vector to the void surface, as shown in Fig. 2a (note that we are employing indicial notation, whereby subscript indices label vector/tensor components and vary from 1 to 3). At a given time step t_n, the following two problems are solved sequentially:

(i) *Deformation without surface diffusion*. Following Needleman and Rice (1980), we construct the integral form of local quasi-static equilibrium using the principle of virtual work in rate form:

$$\iint_A \sigma_{ij}\delta\dot{\varepsilon}_{ij}dA = \int_{S_T} T_i\delta v_i ds - \int_{S_s} \gamma_s\kappa\delta v_n ds - \int_{S_b} \sigma_n\delta v_n ds, \tag{10}$$

where σ_{ij} is the Cauchy stress field, δv_i is a virtual velocity field, $\delta\dot{\varepsilon}_{ij} = \mathrm{sym}(\delta v_{i,j})$ is the associated virtual strain rate field (a comma in a subscript denotes a spatial gradient: $(\cdot)_{,j} = \partial(\cdot)/\partial x_j$), T_i is the applied traction on S_T, and $\delta v_n = \delta v_i n_i$ (note that we are employing the Einstein summation convention, whereby it is understood that repeated indices are summed over from 1 to 3). The negative signs result from the normality convention employed here, that the normal vector is taken to point *into* the material on both S_s and S_b; again, this is done to maintain consistency with Needleman and Rice (1980). The integral on the left-hand side of (10) represents the rate of virtual work done by internal forces, and the integrals on the right-hand side represent the rates of virtual work done by the forces acting along the boundaries, under the virtual displacement rate δv_i. Equation (10) therefore enforces quasi-static equilibrium of the unit cell under the applied tractions T_i, the normal stress $\gamma_s\kappa$ due to the curvature of the void surface, and the normal stress σ_n along the grain boundary—in short, all processes except surface diffusion.

By finite element discretization, (10) is converted into a set of finite element equations

$$f_i(\Delta u_j) = 0, \tag{11}$$

where the f_i are referred to as the residuals, the Δu_j are the unknown nodal displacement increments, and in this numerical context subscript indices range from 1 to the total number of degrees of freedom (in this case, $2N$, where N is the total number of nodes). The finite element mesh used in the present work is shown in Fig. 2b. A total of 256 eight-noded, biquadratic quadrilateral elements were used. Equation (11) is solved iteratively via the Newton-Raphson method using custom FORTRAN code. Starting from an initial guess for the displacement increments Δu_i, we iterate on the linearized equation

$$K_{ij}\Delta\left(\Delta u_j\right) = -f_i, \tag{12}$$

where

$$K_{ij} = \frac{\partial f_i}{\partial \Delta u_j} \tag{13}$$

is the Jacobian (also known as the global stiffness matrix) and $\Delta\left(\Delta u_i\right)$ are the iterative updates to the initial guess for the displacement increments. Once the residuals have reached zero to within the desired tolerance, the solution is deemed to have converged for the current time step. This yields the displacement increments Δu_i for each node, which determine the *baseline* displacement increments Δu_i^0 for the void surface. Once these are known, the mass flux along the entire grain boundary $j_b(s)$ is evaluated by integrating (8). And since $j_s(s_C) = j_b(s_C)$, the mass flux along the void surface at point C is determined.

(ii) *Matter deposition along the void surface*. Equations (6) and (7) are then solved simultaneously for the rate $\dot{\alpha}$ at which matter is being deposited onto the void surface, and thus the thickness $\Delta\alpha = \dot{\alpha}\Delta t$ deposited during the time increment Δt. Once $\Delta\alpha$ is known, the new shape of the void is constructed according to $\Delta u_i^s = \Delta u_i^0 - \Delta\alpha n_i$. This determines the curvature κ along the entire void surface for use in (10) at the next time step $t_{n+1} = t_n + \Delta t$. Indeed, it is the curvature κ that couples the two problems (i) and (ii).

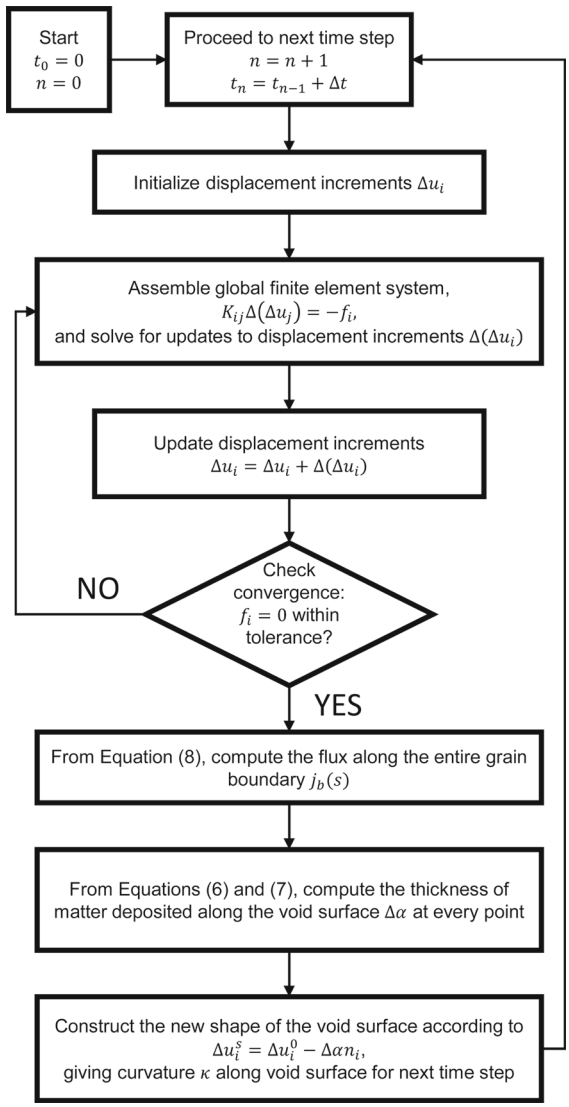

Fig. 3 Block diagram flowchart illustrating the numerical solution algorithm. The full mathematical details can be found in Appendix F of Sanders (2017)

Figure 3 shows a schematic block diagram illustrating the numerical solution algorithm. The full mathematical details of this solution procedure may be found in Appendix F of Sanders (2017).

The constitutive behavior of the grain can be modeled using either classical power-law creep (which only captures secondary creep), or, to investigate the effects of primary creep, a unified creep-plasticity model due to Robinson et al. (1976). In the power-law model, the strain rate tensor is given by

$$\dot{\varepsilon}_{ij} = \dot{\varepsilon}_0 \left(\frac{\sigma_e}{\sigma_0}\right)^n \left(\frac{3}{2}\frac{\sigma'_{ij}}{\sigma_e}\right), \tag{14}$$

where $\dot{\varepsilon}_0 = 10^{-6}\ \mathrm{s}^{-1}$ is the conventional reference strain rate, σ_0 is the reference stress, n is the creep exponent, a subscript e denotes a von Mises equivalent quantity such that, for any tensor T_{ij},

$$T_e = \sqrt{\tfrac{3}{2} T'_{ij} T'_{ij}}, \tag{15}$$

a prime denotes the deviatoric part of a tensor such that $T'_{ij} = T_{ij} - \frac{1}{3} T_{kk}\delta_{ij}$, and δ_{ij} is the Kronecker delta. The Robinson–Pugh–Corum model (Robinson et al. 1976) (henceforth referred to as the "RPC model") accounts for both primary and secondary creep, with a smooth transition between the two. In this model, the strain rate tensor is given by

$$\dot{\varepsilon}_{ij} = A\,\Sigma_e^{\,m} \left(\frac{3}{2}\frac{\Sigma'_{ij}}{\Sigma_e}\right), \tag{16}$$

where the scalars A and m are temperature-dependent material parameters, and the effective stress $\Sigma_{ij} = \sigma_{ij} - \alpha_{ij}$ is the difference between the local Cauchy stress tensor σ_{ij} and the local flow stress tensor α_{ij}. The flow stress α_{ij} is an internal state variable, similar to the kinematic hardening variable of classical plasticity theory, which represents the local material microstructure in that $\alpha_e = B\sqrt{\rho}$, where B is another temperature-dependent material parameter and ρ is the local dislocation density. The time-dependence of the flow stress is governed by the following evolution equation:

$$\dot{\alpha}_{ij} = \frac{2C}{3\alpha_e}\dot{\varepsilon}_{ij} - D\alpha_e^{\,2}\alpha_{ij}, \tag{17}$$

where C and D are additional temperature-dependent material parameters. As discussed in detail by Sanders et al. (2020), the first and second terms on the right-hand side of (17) represent strain hardening and recovery of the material, respectively. It is the competition between strain hardening and recovery that brings about the transition from primary to secondary creep, which is characterized by the time scale

$$\tau = \frac{1}{\sqrt{ACD\left(S - B\sqrt{\rho_0}\right)^m}}, \tag{18}$$

where ρ_0 is the initial dislocation density (Sanders et al. 2020). By comparing the results obtained using the power-law model and the RPC model (Robinson et al. 1976), it is possible to see directly the effects of primary creep on void growth.

Table 1 Approximate chemical composition of 2 1/4 Cr-1 Mo steel (Sanders et al. 2020)

C	Cr	Fe	Mn	Mo	P	S	Si
0.05–0.15	2.0–2.5	Bal.	0.3–0.6	0.9–1.1	0.025	0.025	0.5

All values are percentage by mass

3 Simulation results

To be definite, we will consider material parameters representative of 2 1/4 Cr-1 Mo Steel at 566 °C (Robinson et al. 1976), the limiting chemical composition of which can be found in Table 1. As noted by Sanders et al. (2020), at 566 °C this alloy exhibits a significant primary creep phase, making it an excellent candidate to investigate the effects of primary creep on void growth. From experimental creep test data reported by Robinson et al. (1976), we find that, with $\dot{\varepsilon}_0 = 10^{-6}\,\mathrm{s}^{-1}$, the power-law reference stress and creep exponent are $\sigma_0 \approx 550$ MPa and $n \approx 4.4$, respectively. Typically, during tensile tests, the applied stress S does not exceed the power-law reference stress σ_0, and here we will fix the applied stress at $S = 100$ MPa, which is less than σ_0 but still of the same order of magnitude. Additionally, Robinson et al. (1976) give the following material parameters for the RPC model: $A = 4.87 \times 10^{-40}\,\mathrm{Pa}^{-4}\,\mathrm{s}^{-1}$, $B = 8.76\,\mathrm{Pa\,m}$, $C = 7.9031 \times 10^{17}\,\mathrm{Pa}^2$, $D = 2.382 \times 10^{-23}\,\mathrm{Pa}^{-2}\,\mathrm{s}^{-1}$, $m = 4$, and $\rho_0 = 2.79 \times 10^{11}\,\mathrm{m/m}^3$. With these material parameters and $S = 100$ MPa, the transition time between primary and secondary creep comes out to about $\tau = 320$ h.

To generalize our results to other materials at other temperatures, we will report all results in terms of the dimensionless groups given in (5). Experimental micrographs of 2 1/4 Cr-1 Mo Steel (Klueh and Swindeman 1983) reveal that the local void distribution can vary dramatically, even within the same sample. The size of an individual void can be anywhere from a fraction of a micron to one micron in diameter, and the void spacing can range from a fraction of a micron to several microns. Here, as in Sanders et al. (2021), we will consider an initial void radius of $a_0 = 1\,\mu\mathrm{m}$ and an initial half-spacing of $b = 10\,\mu\mathrm{m}$, fixing the initial porosity $a_0/b = 0.1$. Based on data reported in Frost and Ashby's celebrated deformation mechanism maps (Frost and Ashby 1982), we estimate that, for 2 1/4 Cr-1 Mo Steel at 566 °C, $\mathcal{D}_b \sim 5 \times 10^{-33}\,\mathrm{m}^6/\mathrm{J\,s}$. Using these values, we estimate that $L_b/a_0 \sim 10$, and we will consider values of L_b/a_0 in this neighborhood. Recall that, according to Needleman and Rice (1980), grain boundary diffusion and bulk creep exert comparable influence on void growth for values of L_b/a_0 between 4 and 20, so we expect to see the influence of both mechanisms in our simulations. As for L_s/a_0, we will consider values up to 80, which we will see is sufficient to observe both quasi-equilibrium and crack-like void growth. For metals at high temperatures, $\gamma_s \sim 0.5\,\mathrm{J/m}^2$ Chattopadhyay (2001), so with $S = 100$ MPa, we have that $Sa_0/\gamma_s \sim 200$, and we will consider values on that order of magnitude or less.

It will prove instructive to begin with results obtained using the classical, power-law creep model, which only accounts for secondary creep. Figure 4 shows representative results for model parameters $L_s/a_0 = 20, 40, 60$, $L_b/a_0 = 8$, $Sa_0/\gamma_s = 200$, $a_0/b = 0.1$, and $\psi = \pi/2$, illustrating the effect of increasing the normalized surface diffusion length while holding all other parameters fixed. Figure 4a, c, and e show the void profiles at various times, while Fig. 4b, d, and f show the corresponding mass flux distributions along both the void surface and the grain boundary. All times are normalized by the RPC transition time $\tau = 320$ h (this is done in order to facilitate comparison with the RPC model later), the flux is normalized by a reference flux

$$j_{\mathrm{ref}} = \frac{3\mathcal{D}_b S b}{(b - a_0)^2}, \tag{19}$$

and the arc length s is normalized by its maximum value at point D. As is evident from Fig. 4, the reference flux j_{ref} gives a good estimate of the flux at the intersection between the void surface and the grain boundary (point C in Fig. 2a).

Figure 4a shows the simulated void profiles for $L_s/a_0 = 20$. The data points indicate the locations of individual nodes along the void surface. In this case, the void only expands in the x-direction (the direction parallel to the grain boundary), which is the hallmark of crack-like void growth. From Fig. 4b, it can be seen that the mass flux along the void surface is negative near the top of the void—between $s/s_{\max} = 0$ and $s/s_{\max} \approx 0.1$—and positive elsewhere. Furthermore,

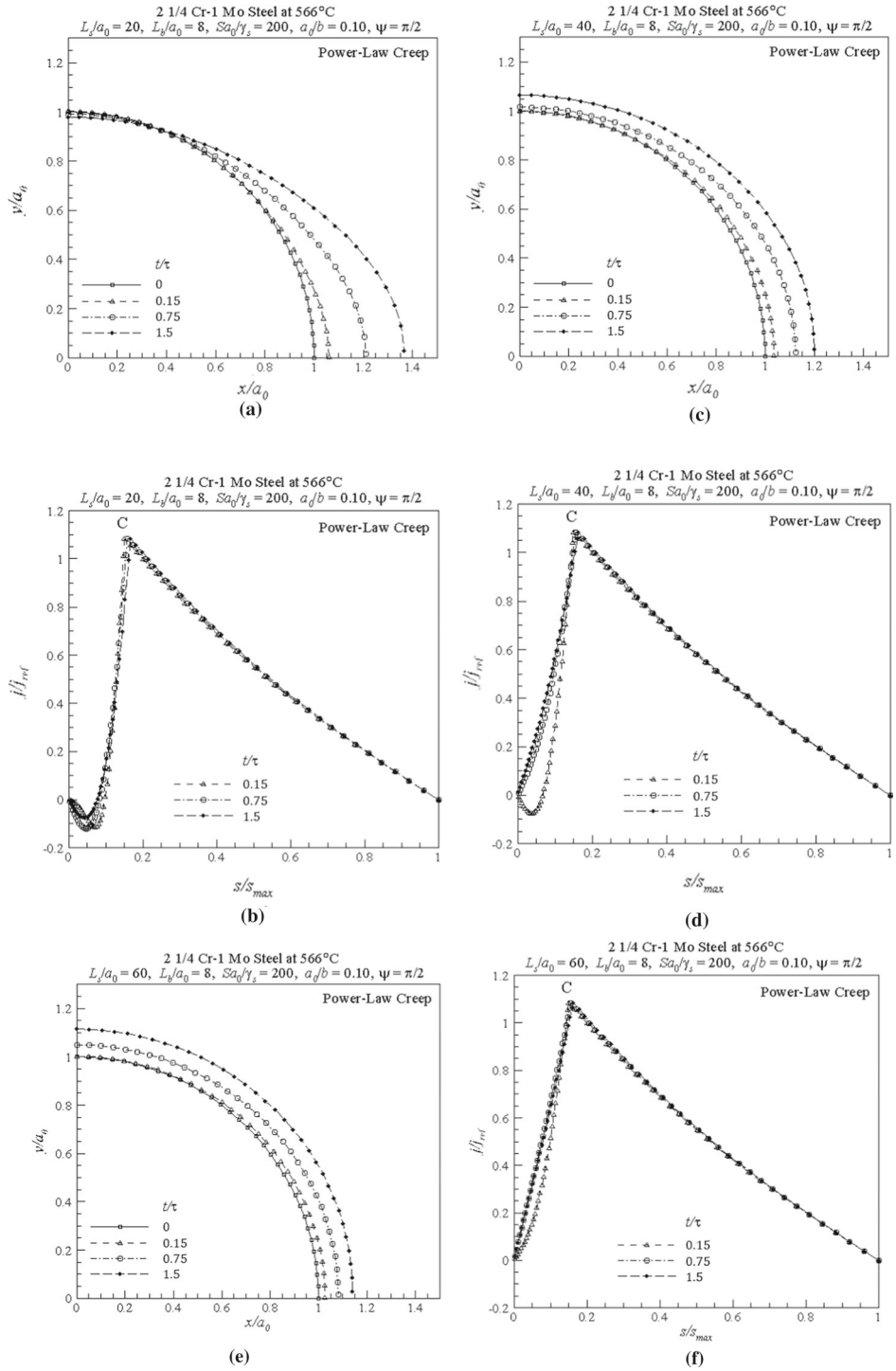

Fig. 4 Simulated void shape profiles and mass flux distributions at various nondimensionalized times for given values of the dimensionless groups L_s/a_0, L_b/a_0, Sa_0/γ_s, a_0/b, and ψ, obtained using the power-law creep model. **a** and **b** Crack-like void growth. **c** and **d** Dynamic void growth. **e** and **f** Quasi-equilibrium void growth

the flux initially decreases with arc length, achieving a local minimum at $s/s_{\max} \approx 0.05$, before increasing up to its maximum value $j/j_{ref} \approx 1.1$ at the void tip. According to (6), this means that $\dot{\alpha}$ is positive near the top of the void, and negative near the void tip. That is, matter is being deposited onto the void surface at the top of the void, but it is being depleted from the void surface near the grain boundary. It is the deposition of matter at the top of the void that prevents the void from expanding in the y-direction.

Figure 4c shows the void profiles for $L_s/a_0 = 40$. In this case, there is some expansion in the y-direction, so it cannot be said that the void growth is truly crack-like. However, the expansion in the x-direction is more pronounced than that in the y-direction, so it cannot be said that the void growth is truly quasi-equilibrium either. Examination of the flux in Fig. 4d reveals that, at time $t/\tau = 0.15$, the qualitative behavior is similar to that in Fig. 4b, in that there is deposition of matter near the top of the void. However, by time $t/\tau = 0.75$, the flux along the void surface is everywhere positive and increasing. At that and all subsequent times, matter is only ever depleted from the void surface, never deposited. We will refer to such behavior as "dynamic" void growth, which we identify with the region of overlap in Kagawa's (1976) and Chuang et al.'s (1979) criteria, as discussed in Sect. 1.

Finally, Fig. 4e shows the void profiles for $L_s/a_0 = 60$. In this case, the amount of expansion in the x-direction is nearly the same as that in the y-direction. From Fig. 4f, the flux along the void surface is everywhere positive and increasing for all times shown, indicating that matter is only ever depleted from the void surface. This is the hallmark of quasi-equilibrium void growth. Thus, by accounting explicitly for both surface and grain boundary diffusion, the present model is able to capture both crack-like and quasi-equilibrium void growth, depending on the system parameters—in particular the normalized diffusion lengths L_s/a_0 and L_b/a_0.

We pause here to observe that labeling the behavior of a given simulation as either "crack-like" or "quasi-equilibrium" is, to some extent, artificial. This is perhaps most evident from the behavior of the surface flux near the top of the void. It could be argued from our discussion of Fig. 4 that crack-like void growth is associated with there being a region near the top of the void in which the mass flux is negative, so that matter is deposited near the top of the void. If we use that as the criterion for crack-like void growth, then we would conclude that Fig. 4c actually exhibits a *transition* from crack-like void growth at small times to quasi-equilibrium void growth at large times. It may very well be that all void growth is what we have called "dynamic," transitioning from crack-like to quasi-equilibrium, with the duration of the crack-like phase longer or shorter, depending on the system parameters. When we say that the behavior of a given simulation is "crack-like," then, we mean that the duration of the crack-like phase is significant. In general, for a fixed value of the grain boundary diffusion length L_b/a_0, the duration of crack-like void growth decreases as the surface diffusion length L_s/a_0 increases, until it is no longer noticeable. Indeed, there is barely any crack-like growth noticeable in Fig. 4e, which we have appropriately labeled as "quasi-equilibrium." This makes sense, and is consistent with the well-known result that when surface diffusion occurs much more rapidly than grain boundary diffusion, the void exhibits quasi-equilibrium void growth (Chuang et al. 1979; Kagawa 1976; Needleman and Rice 1980).

3.1 Effect of primary creep on void growth

To see the effects of primary creep, we exchange the power-law creep model in favor of the RPC model (Robinson et al. 1976). Figure 5 shows analogous plots to Fig. 4, using the RPC model instead of power-law creep. The only difference between these two sets of figures is the constitutive model used; all of the other model parameters remain the same between each pair of corresponding figures. In computing the diffusion lengths L_s and L_b for the RPC model, we are setting $n = m$ and $\sigma_0 = (\dot{\varepsilon}_0/A)^{1/m}$. The qualitative behavior of the void profile and the mass flux is essentially the same for RPC creep as it was for power-law creep—indeed, it is rather remarkable how similar the shapes of the plots are. It would seem that primary creep does not affect the actual shapes assumed by the void as it grows. However, there is one major difference. In Fig. 5, by time $t/\tau = 0.018$, the void has already reached the same size and shape as it did by time $t/\tau = 1.5$ in Fig. 4. Apparently, when primary creep is accounted for, the void initially grows about $1.5/0.018 \approx 83$ times faster than it does when primary creep is neglected. We note that this same "acceleration factor" of 83 was observed for all simulations performed with an applied

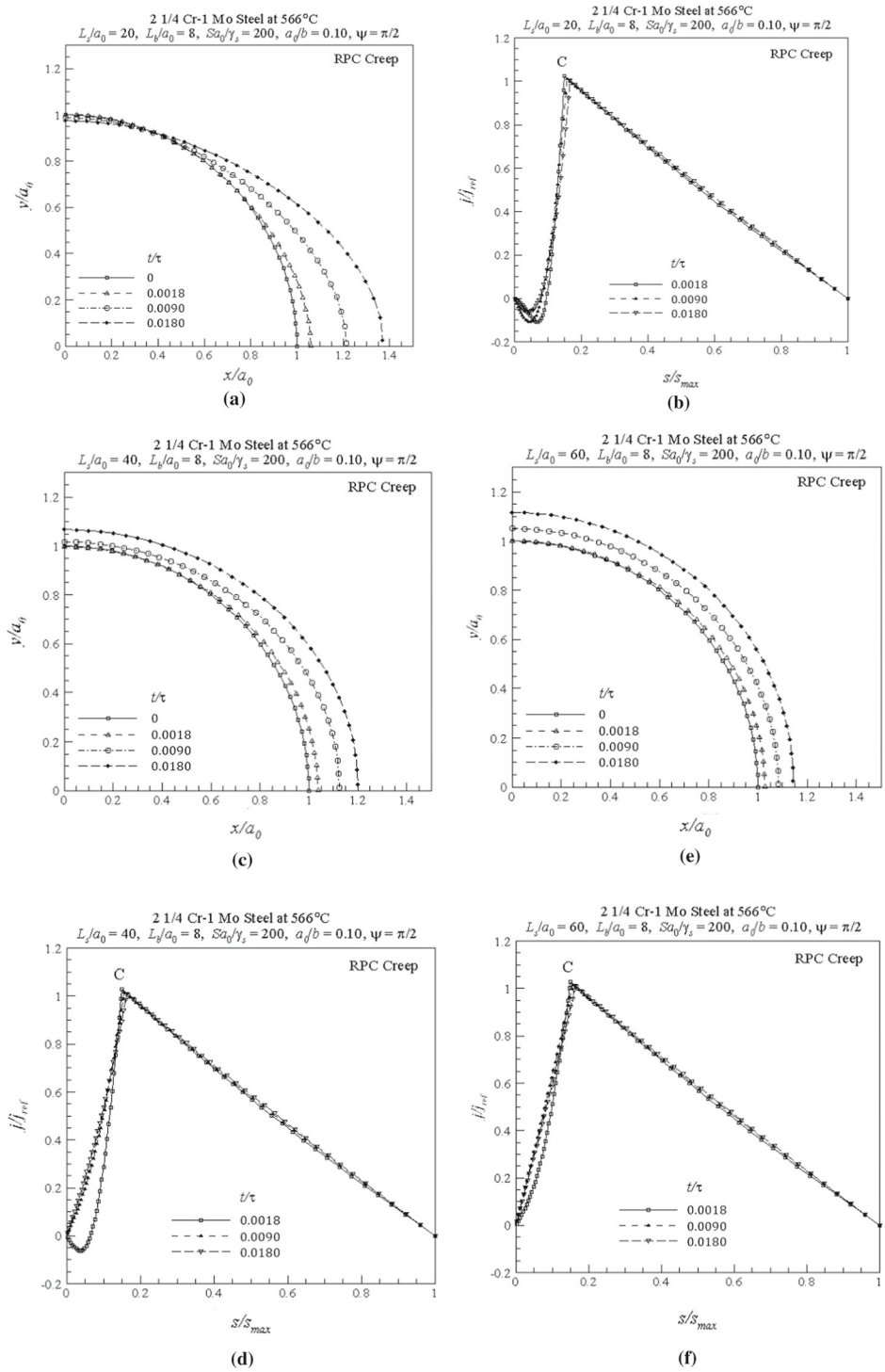

Fig. 5 Simulated void shape profiles and mass flux distributions at various nondimensionalized times for given values of the dimensionless groups L_s/a_0, L_b/a_0, Sa_0/γ_s, a_0/b, and ψ, obtained using the RPC creep model (Robinson et al. 1976). **a** and **b** Crack-like void growth. **c** and **d** Dynamic void growth. **e** and **f** Quasi-equilibrium void growth

tensile stress $S = 100$ MPa, regardless of the values of L_b/a_0, L_s/a_0, and Sa_0/γ_s. This is to be expected, since the strain rate is higher in the primary creep phase than in the secondary creep phase. Hence, we expect to see the void grow faster when primary creep is accounted for, compared to when primary creep is neglected.

The acceleration factor ξ (here, 83 for material parameters representative of 2 1/4 Cr-1 Mo Steel at 566°C with $S = 100$ MPa) can be estimated based on the applied stress S and the material parameters. One estimate is given by

$$\xi_- = \frac{A\left(S - B\sqrt{\rho_0}\right)^m}{\dot{\varepsilon}_0 \left(S/\sigma_0\right)^n} \sim 73. \tag{20}$$

This is simply the ratio between the initial strain rate (i.e., at time $t = 0$) predicted by the RPC model and the strain rate predicted by the power-law creep model in a uniaxial creep test with remotely applied stress S. As the subscript is meant to suggest, it would appear that (20) gives a lower-bound estimate, since the actual acceleration factor here is 83. A slightly higher estimate can be obtained by omitting the factor of $B\sqrt{\rho_0}$ in (20) as follows:

$$\xi_+ = \frac{AS^m}{\dot{\varepsilon}_0 \left(S/\sigma_0\right)^n} \sim 88. \tag{21}$$

The above appears to give an upper-bound estimate for the acceleration factor. In any case, the fact that the true acceleration factor falls between these two estimates suggests that the void growth rate scales with the remote strain rate (at least approximately).

3.2 Criteria for quasi-equilibrium and crack-like void growth

To establish quantitative criteria for quasi-equilibrium versus crack-like void growth, we have performed a parametric study on the dimensionless groups $L_b/a_0 \in [7, 13]$, $L_s/a_0 \in [20, 80]$, and $Sa_0/\gamma_s \in \{50, 100, 150, 200\}$ (recall that we have fixed $a_0/b = 0.10$ and $\psi = \pi/2$). In total, over 286 simulations have been performed [half with the power-law model and half with the RPC model (Robinson et al. 1976)], and each simulation was categorized as primarily quasi-equilibrium, crack-like, or dynamic. The void growth was categorized as quasi-equilibrium if the void grew the same amount ($\pm 0.05a_0$) in both the x- and y-directions during the entire course of the simulation; crack-like if the void grew at least $0.20a_0$ in the x-direction without growing more than $0.05a_0$ in the y-direction during the entire course of the simulation; and dynamic otherwise. We note that the two constitutive models yielded identically shaped void profiles for every set of parameters considered here, the only difference being the acceleration factor of 83 noted above. Figure 6 summarizes the results.

Note that, for fixed values of Sa/γ_s, a/b, and ψ, and with Kagawa's (1976) suggested cutoff value of $\chi_0 = 5$, Kagawa's (1976) criteria, as given by (2) and (3), define lines that separate the L_bL_s-plane into three regions, corresponding to quasi-equilibrium, crack-like, and dynamic void growth. For example, with $Sa/\gamma_s = 100$, $a/b = 0.10$, and $\psi = \pi/2$, (2) and (3) imply that quasi-equilibrium void growth should occur for $L_s/L_b > 1.58$, crack-like void growth for $L_s/L_b < 1.52$, and dynamic void growth for $1.52 < L_s/L_b < 1.58$. The linear boundaries given by Kagawa's (1976) criteria are illustrated in grey in Fig. 6. Not surprisingly, our results (which account for creep of the grains) do not align with Kagawa's (1976) criteria (which were derived for rigid grains). However, there still appear to be linear boundaries between the regions of crack-like, quasi-equilibrium, and dynamic void growth defined by the data points in Fig. 6. This suggests that the void shape may still depend on L_s and L_b only in their ratio, even when creep is accounted for. That is, the void shape may be a function of just four dimensionless groups (L_s/L_b, Sa_0/γ_s, a_0/b, and ψ), not the five dimensionless groups (5) identified using dimensional analysis.

Boundaries consistent with the present results are illustrated in black in Fig. 6. For example, with $Sa/\gamma_s = 100$, we find that the quasi-equilibrium region is well approximated by the condition $L_s/L_b > 5.63$, and that the crack-like region is well approximated by the condition $L_s/L_b < 3.05$. Note that, in all cases, our threshold values for L_s/L_b are *higher* than the corresponding values given by Kagawa (1976). In other words, for a fixed value of L_b, L_s must be *greater* in the presence of bulk creep than in the case of rigid grains in order to bring about quasi-equilibrium void growth. This suggests that crack-like void growth may be more common than previously thought at high temperatures.

Our threshold values of L_s/L_b for crack-like and quasi-equilibrium void growth are plotted against Sa_0/γ_s in Fig. 7a. Interestingly, these plots are also approximately linear, with both linear trend lines exhibiting determination coefficients (r^2) in the neigh-

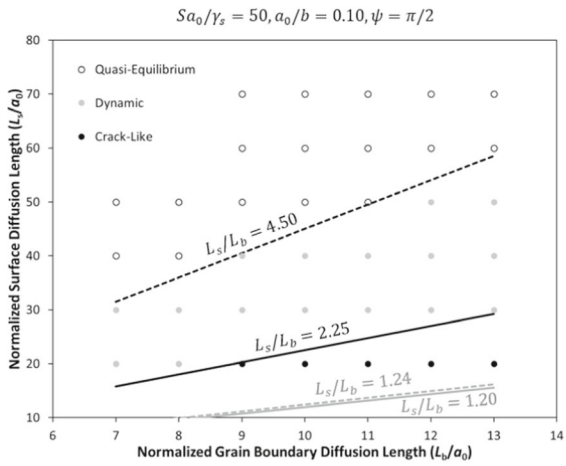

Fig. 6 Summary of simulation results for $Sa_0/\gamma_s =$ **a** 50, **b** 100, **c** 150, and **d** 200, with $a_0/b = 0.10$ and $\psi = \pi/2$. Each data point represents a single simulation using the given values of L_s/a_0 and L_b/a_0, and the points are shaded based on the void shape observed: quasi-equilibrium (white), dynamic (grey), or crack-like (black). The grey lines represent the criteria derived by Kagawa (1976) for rigid grains using nominal values $a/b = 0.10$ and $\chi_0 = 5$ in (2) and (3). The black lines represent criteria consistent with our results, which account for bulk creep in the grains

borhood of 0.91. Thus, the following criteria for quasi-equilibrium and crack-like void growth give an approximate representation of the results presented in this work:

quasi-equilibrium void growth:

$$\frac{L_s}{L_b} > 0.0121\left(\frac{Sa_0}{\gamma_s}\right) + 4.065, \tag{22}$$

crack-like void growth:

$$\frac{L_s}{L_b} < 0.0131\left(\frac{Sa_0}{\gamma_s}\right) + 1.575. \tag{23}$$

For a more direct comparison to Kagawa's (1976) criteria, we may invert the ordinates and abscissae in Fig. 7a, obtaining Fig. 7b and the following criteria:

quasi-equilibrium void growth:

$$\frac{Sa_0}{\gamma_s} < -292.38 + 74.766\left(\frac{L_s}{L_b}\right), \tag{24}$$

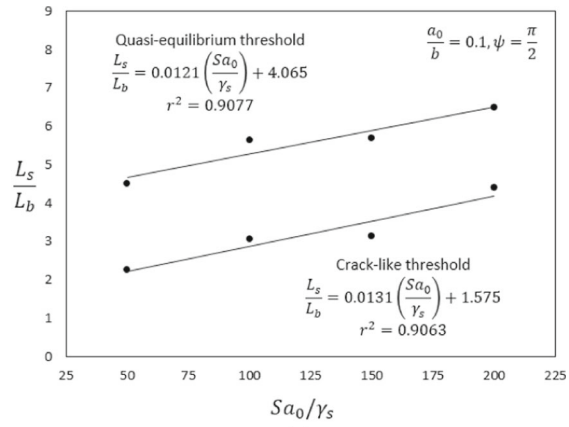

(a)

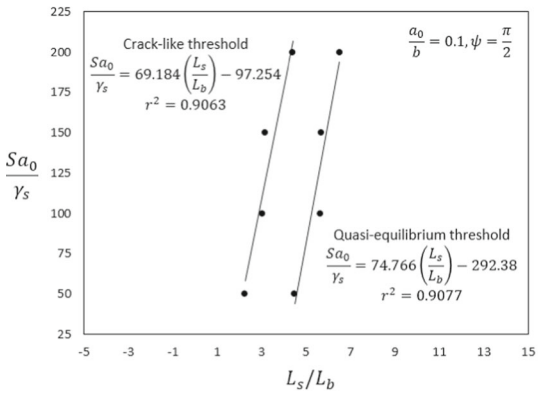

(b)

Fig. 7 Observed thresholds for quasi-equilibrium and crack-like void growth with $a_0/b = 0.1$ and $\psi = \pi/2$, consistent with the results shown in Fig. 6, along with linear trend lines. **a** L_s/L_b plotted against Sa_0/γ_s. **b** Sa_0/γ_s plotted against L_s/L_b

crack-like void growth:

$$\frac{Sa_0}{\gamma_s} > -97.254 + 69.184\left(\frac{L_s}{L_b}\right). \tag{25}$$

We emphasize that the above criteria were developed to approximate our numerical results (which account for creep of the grains), and we do not expect our criteria to match Kagawa's (1976) criteria (which were derived for rigid grains). Nevertheless, it is interesting to compare (24) and (25) to (2) and (3), respectively. Despite a superficial resemblance, we note two important differences. The first is that the ratio L_s/L_b appears linearly in (24) and (25) but cubically in (2) and (3), since $\Delta = (L_s/L_b)^3$. The second difference is the sign of the remaining terms, which are negative in (24) and (25) but positive in (2) and (3). It should be noted, however, that our criteria are consistent with Kagawa's (1976) criteria in certain extreme limits. For both sets of criteria, when grain boundary diffusion is negligible (mathematically, when the ratio L_s/L_b is taken to infinity with all other parameters held fixed), the possibility of crack-like void growth is excluded; and when surface tension is negligible (mathematically, when Sa_0/γ_s is taken to infinity with all other parameters fixed), the possibility of quasi-equilibrium void growth is excluded. Interestingly, our criteria are *not* consistent with Kagawa's (1976) criteria when surface diffusion is negligible (mathematically, when L_s/L_b is taken to zero with all other parameters held fixed). In that case, the possibility of quasi-equilibrium void growth is excluded under our criteria (as it should be), but Kagawa's (1976) criteria allow for both quasi-equilibrium and crack-like void growth in that limit. This lends some physical plausibility to our criteria. However, we are quick to emphasize that the criteria given by (22)–(25) were developed specifically for dimensionless parameter values $L_b/a_0 \in [7, 13]$, $L_s/a_0 \in [20, 80]$, $Sa_0/\gamma_s \in [50, 200]$, $a_0/b = 0.10$, and $\psi = \pi/2$. Caution should be taken when extrapolating to other values.

4 Discussion and conclusion

We may summarize the present results with the following two observations:

1. Crack-like void growth appears to be more prevalent at high temperatures than previously assumed based on rigid-grain models. This is evident from Fig. 6, where the thresholds for crack-like void growth are higher than those given by Kagawa (1976). In other words, the region of crack-like void growth is larger in the presence of bulk creep than would be predicted assuming rigid-grains.
2. Void growth of any kind is substantially accelerated during the primary creep phase. In all 286 simulations carried out for the present work, regardless of the system parameters, the void grew significantly faster in the presence of primary creep than would be expected based on the power-law creep model, although the actual shapes assumed by the void were not affected by the presence of primary creep. The "acceleration factor" (here, 83 for material parameters representative of 2 1/4 Cr-1 Mo Steel at 566 °C with an applied uniaxial stress

of $S = 100$ MPa) was found to be in good agreement with estimates (20) and (21) based on the ratio between the strain rates in the primary and secondary creep phases, suggesting that the void growth rate scales (at least approximately) with the remote strain rate.

These observations could have serious implications for previous creep cavitation models. Recall that, because Needleman and Rice (1980) did not model the surface diffusion process explicitly, their model could not anticipate or simulate crack-like void growth, and they did not account for primary creep. It is possible that creep cavitation models based on the extension of Needleman and Rice (1980) to higher triaxialities (Bieberdorf et al. 2021; Rovinelli et al. 2021; Sham and Needleman 1983; Van der Giessen and Tvergaard 1996; Van der Giessen et al. 1995; Wen et al.'s 2018, 2017) and internal void pressures (Dadfarnia et al. 2019; Van der Burg and Van der Giessen 1996a, b, 1997; Van der Burg et al. 1996) are *underestimating* the true rate of void growth in actual structures and components. The worst-case scenario would be when crack-like void growth occurs during the primary creep phase. In that case, these two effects would compound, and previous models could potentially underestimate the rate of void growth by more than two orders of magnitude, depending on the material and the applied loads. In such cases, any component lifetime estimates that were based on the previous models would be unreliable.

For remote uniaxial tension, the criteria summarized in Fig. 6 and approximated by (22)–(25) can be used to estimate whether or not crack-like void growth will occur for a given material at a given temperature under given loading conditions (within the limits set by the parameters considered here). As long as only quasi-equilibrium void growth occurs, our results suggest that previous models may be corrected by simply scaling the void growth rate $\dot{a}$ by an acceleration factor ξ given by

$$\xi \approx \frac{\dot{\varepsilon}_\infty(t)}{\dot{\varepsilon}^*_\infty}, \tag{26}$$

where $\dot{\varepsilon}_\infty(t)$ is the current remote uniaxial strain rate at any given time, and $\dot{\varepsilon}^*_\infty$ is the remote uniaxial strain rate during secondary creep. The previous models cannot be so corrected when crack-like or dynamic void growth is present. In that case, additional modeling will be necessary.

Funding No funds, grants, or other support was received.

Code Availability The authors retain all intellectual property rights to the custom code used in the present work. This code is proprietary and will therefore not be shared.

Declarations

Conflict of interest The authors declare that they have no conflicts of interest.

References

Argon AS (1982) Mechanisms and mechanics of fracture in creeping alloys. In: Wilshire B, Owen DRJ (eds) Recent advances in creep and fracture of engineering materials and structures. Pineridge Press, Swansea, pp 1–52

Bieberdorf N, Tallman A, Kumar MA, Taupin V, Lebensohn RA, Capolungo L (2021) A mechanistic model for creep lifetime of ferritic steels: application to Grade 91. Int J Plast 147:103086

Budiansky B, Hutchinson JW, Slutsky S (1982) Void growth and collapse in viscous solids. In: Hopkins HG, Sewell MJ (eds) Mechanics of solids: the Rodney Hill 60th anniversary volume. Elsevier, Amsterdam, pp 607–652

Chattopadhyay R (2001) Surface wear: analysis, treatment, and prevention. ASM International, Materials Park

Chen IW, Argon AS (1981) Diffusive growth of grain-boundary cavities. Acta Metall 29:1759–1768

Chersola D, Lomonaco G, Marotta R (2015) The VHTR and GFR and their use in innovative symbiotic fuel cycles. Prog Nucl Energy 83:443–459

Chuang TJ, Rice JR (1973) The shape of intergranular creep cracks growing by surface diffusion. Acta Metall 21:1625–1628

Chuang TJ, Kagawa KI, Rice JR, Sillis LB (1979) Non-equilibrium models for diffusive cavitation of grain interfaces. Acta Metall 27:265–284

Dadfarnia M, Martin ML, Moore DE, Orwig SE, Sofronis P (2019) A model for high temperature hydrogen attack in carbon steels under constrained void growth. Int J Fract 219:1–17

Frost HJ, Ashby MF (1982) Deformation-mechanism maps: the plasticity and creep of metals and ceramics. Pergamon Press, Oxford

GEN IV International Forum (2020) Annual Report 2020. Tech. rep., GEN IV International Forum. https://www.gen-4.org/gif/jcms/c_178286/gif-2020-annual-report

Huang L, Sauzay M, Cui Y, Bonnaille P (2021) Theoretical and experimental study of creep damage in alloy 800 at high temperature. Mater Sci Eng A 813:140953

Hull D, Rimmer DE (1959) The growth of grain-boundary voids under stress. Philos Magn 4:673–687

Kagawa KI (1976) Models of slow intergranular void growth due to void surface and grain boundary self-diffusion. Master's thesis, Brown University

Klueh RL, Swindeman RW (1983) Mechanical properties of a modified 2 1/4 Cr-1 Mo steel for pressure vessel applications. Tech. rep., Oak Ridge National Laboratory. ORNL-Report TM-5995

Needleman A, Rice JR (1980) Plastic creep flow effects in the diffusive cavitation of grain boundaries. Acta Metall 28:1315–1332

Pan J, Cocks ACF (1995) A numerical technique for the analysis of coupled surface and grain-boundary diffusion. Acta Metall Mater 43(4):1395–1406

Pataky GJ, Sehitoglu H, Maier HJ (2013) Creep deformation and mechanisms in Haynes 230 at 800 C and 900 C. J Nucl Mater 443:484–490

Robinson DN, Pugh CE, Corum JM (1976) Constitutive equations for describing high-temperature inelastic behavior of structural alloys. In: Proceedings of Specialist Meeting on High-Temperature Structural Design Technology of LMFBRs, IAEA Report IWGFR/11

Rovinelli A, Messner MC, Parks DM, Sham TL (2021) Accurate effective stress measures: predicting creep life for 3D stresses using 2D and 1D creep rupture simulations and data. Integr Mater Manuf Innov 10:627–643

Sanders JW (2017) Modeling and simulation of creep rupture in high-temperature alloys. Ph.D. thesis, The University of Illinois at Urbana-Champaign

Sanders JW, Dadfarnia M, Stubbins JF, Sofronis P (2017) On the fracture of high temperature alloys by creep cavitation under uniaxial or biaxial stress states. J Mech Phys Solids 98:49–62

Sanders JW, Dadfarnia M, Sehitoglu H, Stubbins J, Sofronis P (2020) On the stress field ahead of a stationary crack tip during the transition from primary to secondary creep. Int J Solids Struct 193–194:455–473

Sanders J, Jamshidi N, Jamshidi N, Dadfarnia M, Subramanian S, Stubbins J (2021) Simulation of intergranular void growth under the combined effects of surface diffusion, grain boundary diffusion, and bulk creep. In: TMS 2021 150th Annual Meeting & Exhibition Supplemental Proceedings, pp 853–863

Sham TL, Needleman A (1983) Effects of triaxial stressing on creep cavitation of grain boundaries. Acta Metall 31(6):919–926

Subramanian SJ, Sofronis P (2002) Calculation of a constitutive potential for isostatic powder compaction. Int J Mech Sci 44:2239–2262

Sui H, Yu L, Liu W, Liu Y, Cheng Y, Duan H (2022) Theoretical models of void nucleation and growth for ductile metals under dynamic loading: a review. Matter Radiat Extremes 7:018201

Tung HM, Mo K, Stubbins JF (2014) Biaxial thermal creep of inconel 617 and haynes 230 at 850 and 950 C. J Nucl Mater 447:28–37

Tvergaard V (1984) Constitutive relations for creep in polycrystals with grain boundary cavitation. Acta Metall 32:1977–1990

Tvergaard V (1984) On the creep constrained diffusive cavitation of grain boundary facets. J Mech Phys Solids 32:373–393

Tvergaard V (1986) Analysis of creep crack growth by grain boundary cavitation. Int J Fract 31:183–209

Van der Burg MWD, Van der Giessen E (1996a) Hydrogen effects in materials, chap. Hydrogen attack in creeping polycrystals due to cavitation on grain boundaries, pp 313–322

Van der Burg MWD, Van der Giessen E (1996) Non-uniform hydrogen attack cavitation and the role of interaction with creep. Mater Sci Eng A 220:200–214

Van der Burg MWD, Van der Giessen E (1997) A continuum damage relation for hydrogen attack cavitation. Acta Mater 45:3047–3057

Van der Burg MWD, Van der Giessen E, Brouwer RC (1996) Investigation of hydrogen attack in 2.25 Cr-1Mo steels with a high-triaxiality void growth model. Acta Mater 44:505–518

Van der Giessen E, Tvergaard V (1996) Micromechanics of intergranular creep failure under cyclic loading. Acta Mater 44(7):2697–2710

Van der Giessen E, Van der Burg MWD, Needleman A, Tvergaard V (1995) Void growth due to creep and grain boundary diffusion at high triaxialities. J Mech Phys Solids 43(1):123–165

Wen JF, Srivastava A, Benzerga A, Tu ST, Needleman A (2017) Creep crack growth by grain boundary cavitation under monotonic and cyclic loading. J Mech Phys Solids 108:68–84

Wen JF, Liu Y, Srivastava A, Benzerga AA, Tu ST, Needleman A (2018) Environmentally enhanced creep crack growth by grain boundary cavitation under cyclic loading. Acta Mater 153:136–146

World Nuclear Association: Generation IV Nuclear Reactors (2020) World Nuclear Association. https://world-nuclear.org/information-library/nuclear-fuel-cycle/nuclear-power-reactors/generation-iv-nuclear-reactors.aspx